Journal of Power Sources 213 (2012) 47–54

Contents lists available at SciVerse ScienceDirect

Journal of Power Sources

journal homepage: www.elsevier.com/locate/jpowsour

Novel structured electrolytes for solid oxide fuel cells

Bora Timurkutluk [a,b,*], Selahattin Celik [a], Cigdem Timurkutluk [a], Mahmut D. Mat [a], Yuksel Kaplan [a]

[a] HYTEM, Nigde University, Mechanical Engineering Department, 51245 Nigde, Turkey
[b] Vestel Defense Industry, Silicon block, ZK 14, ODTU Teknokent, 06531 Ankara, Turkey

ARTICLE INFO

Article history:
Received 13 January 2012
Received in revised form
29 February 2012
Accepted 9 April 2012
Available online 19 April 2012

Keywords:
Solid oxide fuel cell
Scandia ceria stabilized zirconia
Novel electrolyte

ABSTRACT

Novel grate type electrolytes are designed and fabricated to improve the cell performance and to lower the operation temperature of intermediate temperature electrolyte supported solid oxide fuel cells based on scandium and ceria stabilized zirconia by partly reducing the electrolyte thickness. The characteristics of three different small size cells (11.62 cm^2 active area) having various electrolyte designs are investigated. A standard electrolyte supported cell is also produced as a base case for comparison. Performance measurements showed that all cells having grate type electrolyte produce higher power than that of the base cell due to partly reduced electrolyte thickness. Impedance analysis confirmed that the improvement in the performance is due to the decrease in the electrolyte resistance together with the increased number of active sites. Among the three different designs, Cell C showed the highest power output 14.7 W at 800 °C corresponding to 1.26 W cm^{-2} power density which is more than twice the base case performance.

1. Introduction

A solid oxide fuel cell (SOFC) converts the chemical energy of a fuel directly into electricity without any intermediate energy conversion forms. SOFCs offer environmentally clean, quiet and more efficient operation with fuel flexibility compared to conventional energy conversion systems such as combustion engines. Therefore, in recent years much attention has been given to SOFCs as new generation electricity generating devices. The membrane–electrode assembly (MEA) or positive electrode–electrolyte–negative electrode (PEN) structure is the key element for SOFC systems. PEN structure consists of a solid oxygen ion conducting electrolyte with porous anode and cathode electrodes which include fuel and oxygen catalysts printed on each side, respectively. By the addition of some sort of electrolyte materials in both electrodes, not only the thermal expansion coefficient compatibility between both electrodes and the electrolyte is improved but increase in the number of the reaction sites (three phase boundaries, TPBs) is also achieved improving the cell performance significantly.

A typical SOFC PEN employs yttria stabilized zirconia (YSZ) electrolyte, nickel oxide (NiO)/YSZ anode and lanthanum strontium manganite (LSM)/YSZ cathode. In addition to showing pure ionic conductivity [1–3], YSZ has very good chemical stability [4–6] and good mechanical properties [7–9]. However, YSZ electrolyte supported SOFCs require high operating temperatures around 1000 °C for acceptable performance and ionic conductivity [10,11]. The high operating temperatures of conventional SOFC systems based on YSZ electrolyte (~1000 °C) lead to high production cost due to difficulties in production [12–17], the requirement of special interconnector material and short service life [18]. At such a high temperature that is required for the YSZ electrolyte to achieve adequate ionic conduction, it is difficult to expect a good long-term stability [19–21]. Therefore, the operation temperature of YSZ-based SOFCs should be reduced for cost reduction, long-term operation without degradation and commercialization of SOFC systems.

There exist two ways to lower the operation temperature of SOFCs, i.e. replacing YSZ with alternative electrolyte materials and reducing the YSZ thickness. The first way is to employ an alternative electrolyte material showing the similar properties at relatively low temperatures. Gadolinium/samarium doped ceria (GDC/SDC) and scandium stabilized zirconia (ScSZ) are the most frequent electrolyte materials in this aspect. Although they both show relatively high ionic conductivities, they have some significant drawbacks. GDC/SDC also shows some electronic conductivity resulting in power loss due to short circuiting the cell as well as poor structural stability [22–24] while ScSZ was reported to show phase transition from cubic phase to rhombohedral phase leading to decrease in the ionic conductivity especially below around 650 °C [25–27]. However, Lee et al. [7] and Wang et al. [28] have shown that it is possible to avoid this phase transition by stabilizing the zirconia

* Corresponding author. Vestel Defense Industry, Silicon block, ZK 14, ODTU Teknokent, 06531 Ankara, Turkey. Tel.: +90 388 225 23 37; fax: +90 388 225 01 12.
E-mail address: bora.timurkutluk@nigde.edu.tr (B. Timurkutluk).

0378-7753/$ – see front matter © 2012 Elsevier B.V. All rights reserved.
doi:10.1016/j.jpowsour.2012.04.021

with 1 mol % of ceria along with 10 mol % of scandium. In addition, 10 mol % scandium and 1 mol % ceria stabilized 89 mol % zirconia (ScCeSZ) was reported to show higher ionic conductivities than YSZ at wide temperature ranges [7,29,30]. Therefore, ScCeSZ can be considered as an option for intermediate temperature SOFCs.

The reduction of the electrolyte thickness can be achieved by fabrication of anode/cathode supported PEN designs. However, anode supported SOFCs have the risk of failure due to cycling reduction and oxidation (redox) due to almost inevitable situations during the operation of SOFCs such as seal leakage, fuel supply failure, high fuel utilization or even system shutdown [31–33]. In addition, mass transfer limitations due to thick electrodes can possibly occur in both anode and cathode supported SOFCs. The electrolyte supported design, on the other hand, provides relatively strong structural support and less susceptible to failure due to redox cycling.

Most of the mobile applications require high power density along with a small size. Therefore, the improvement of the cell performance is one of the key issues in the aspects of the extending the range of applications of the SOFC systems. It is possible to increase the SOFC power by effective cell or stack designs. Although there are two main SOFC configurations, i.e. tubular and planar type, there exist several other designs proposed in the literature in order to improve the cell performance by modifying the tubular or planar configuration. There can be found numerous experimental and numerical reports in the literature such as cone-shaped [34–36], flat-tube [37–39], honeycomb [40–42], mono-block-layer-built [43–45] and integrated planar SOFC designs [46–48]. However, most of them relied on standard YSZ-based electrode/electrolyte supported configuration without further modification on the physical properties of the PEN structure specifically the electrolyte thickness.

A typical SOFC electrolyte has a uniform thickness and larger size than the active area for sealing application. In this study, however, novel ScCeSZ-based SOFC electrolytes are designed and fabricated in order to improve the cell performance. Novel electrolytes have grate-like architecture in the active region with a thin support layer in the middle and thick perimeter for ease of sealing and mechanical support. With the benefits of the novel design proposed, a reduction in the operation temperature of SOFCs may also be possible due to partly reduced thickness of the electrolyte in the active area of the cell and increased number of the active sites.

2. Experimental

2.1. Base cell fabrication

The cell comprises mainly three components: anode, electrolyte and cathode. However, each electrode has two different layers namely functional and current collecting layers. Functional layers are the main electrochemical reaction zones while current collecting layers are employed to collect current produced in the cell more effectively. Thus, the cell contains five different layers in total and they are titled from the anode to the cathode side as anode

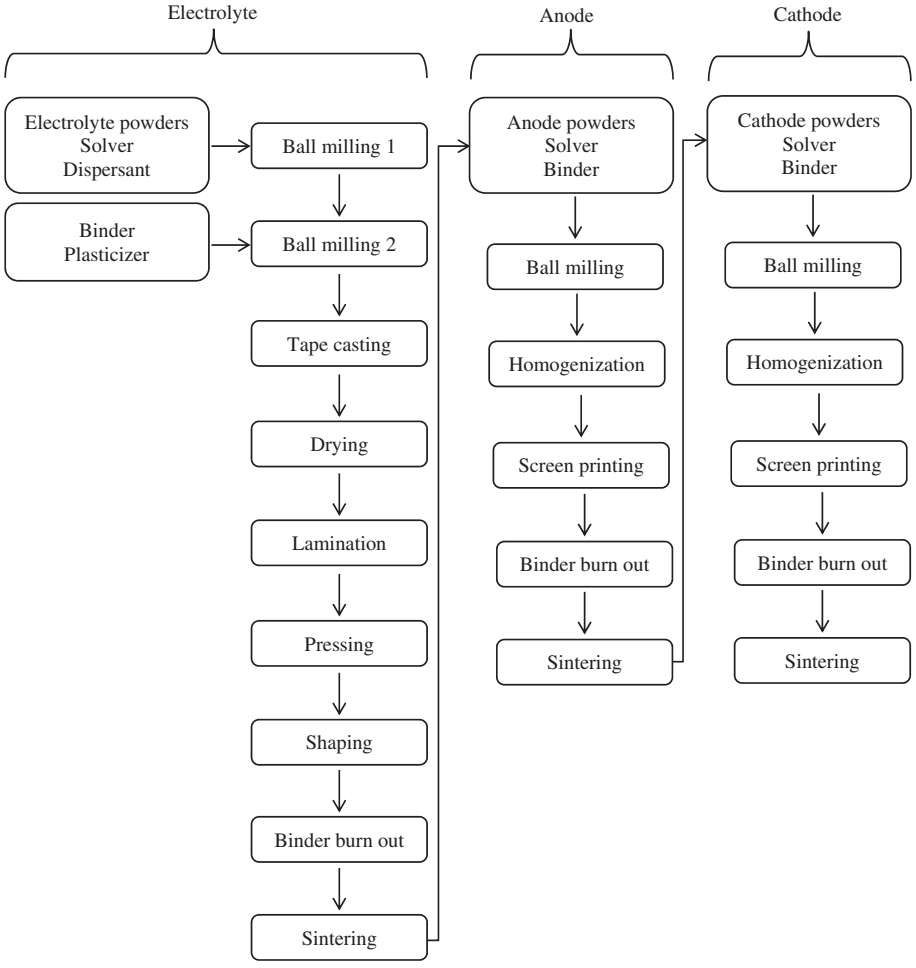

Fig. 1. The flow chart of the cell fabrication.

current collecting layer (ACL), anode functional layer (AFL), electrolyte, cathode functional layer (CFL) and cathode current collecting layer (CCL). The electrolyte is fabricated via tape casting route whereas screen printing technique is used for the fabrication of both electrodes. The cell fabrication process is summarized in Fig. 1.

2.1.1. Electrolyte fabrication for the base cell

High purity ScCeSZ powders ($(Sc_2O_3)_{0.1}(CeO_2)_{0.01}(ZrO_2)_{0.89}$) are purchased from Nextech Materials (Ohio, USA). An alcohol-based tape casting slurry of ScCeSZ is prepared by ball milling at two stages. In the first stage, some certain amount of organic dispersant and solver are added to the ScSZ powders and the mixture is ball milled for around 24 h. In the second stage, organic binder and plasticizer are added with suitable ratios and the ball milling is continued for another 24 h. Then the ScCeSZ slurry is casted on a mylar tape via a laboratory scale tape casting equipment with a blade gap of 170 μm. After drying in atmospheric air for 30 min, the thickness of the green tape is measured as about 35 μm. Six tapes of electrolyte are stacked together and pre-laminated via

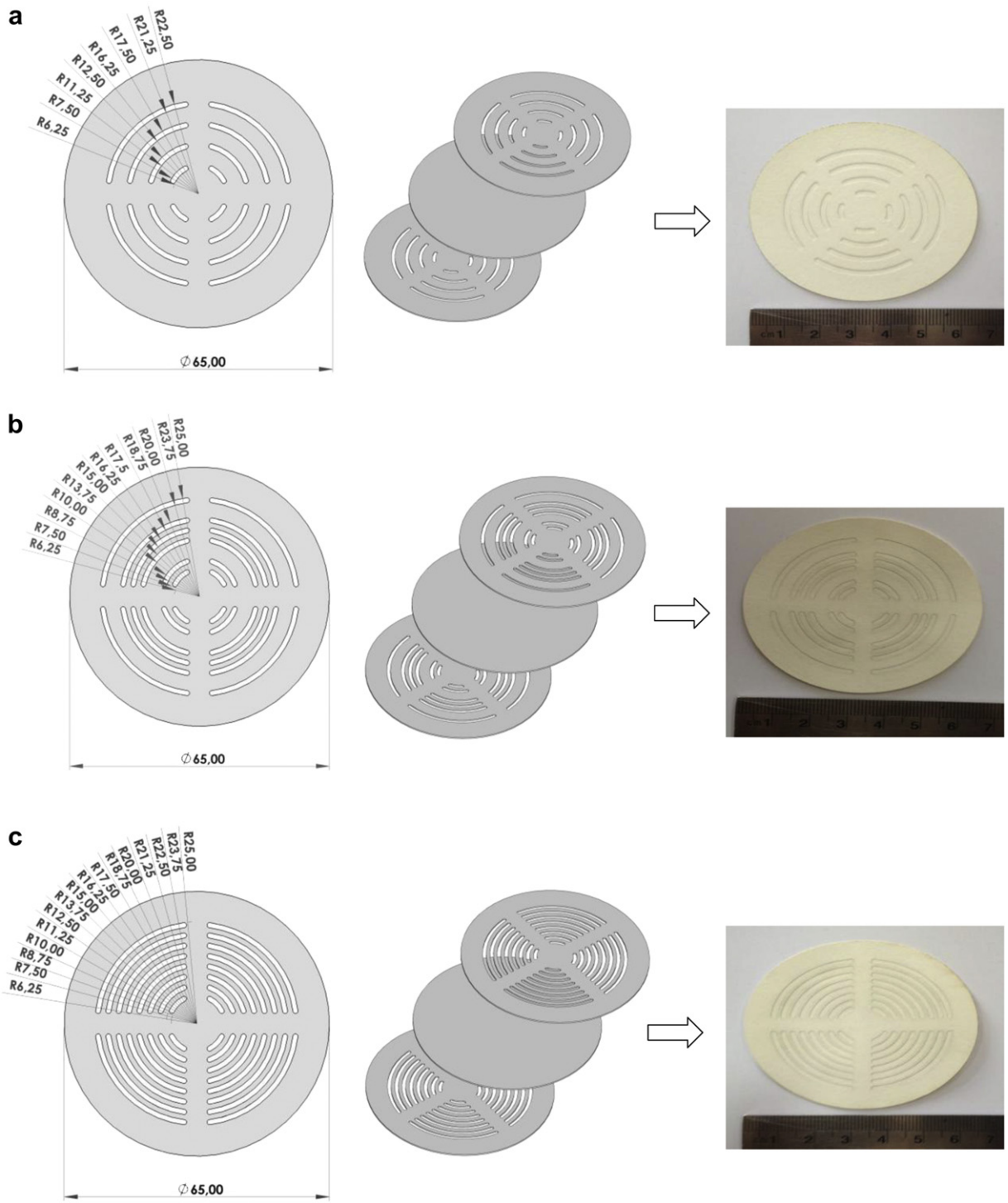

Fig. 2. Technical drawings (left) and photos (right) of novel electrolytes designed for Cell A (a), Cell B (b) and Cell C (c) prior to sintering.

a laboratory scale uniaxial press under 20 MPa pressure for 2 min in order to create an adequate adhesion between tapes before the isostatic pressing step. The laminate is then pressed isostatically under 40 MPa pressure for 10 min. After shaping by a laser cutter in the form of a disc of 65 mm in diameter, ScCeSZ disc is subjected to two different sintering regimes. Firstly, the electrolyte is heated to 1000 °C with 2 °C min^{-1} temperature increment and held for 2 h at this temperature to remove the organic additions. Pre-sintered electrolyte is then moved to the high temperature furnace for the second sintering stage and sintered there at 1400 °C for 5 h with a rate of 3 °C min^{-1} to obtain fully dense electrolyte. The thickness of the base cell electrolyte after sintering is measured as 150 μm whereas the outer diameter of the electrolyte is around 50 mm.

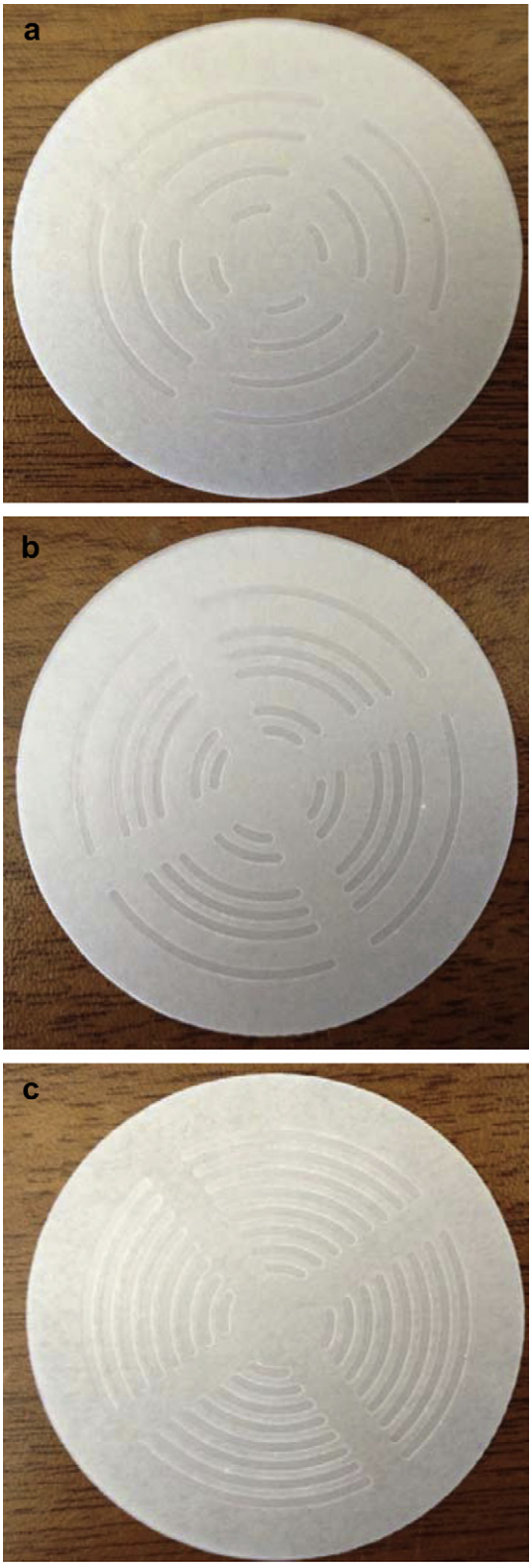

Fig. 3. The photos of electrolytes belonging to Cell A (a), Cell B (b) and Cell C (c) After sintering at 1400 °C for 5 h.

2.1.2. Fabrication of novel electrolytes

Three sets of two layered ScCeSZ electrolyte laminate are fabricated by tape casting and uniaxial pressing similar to the base cell electrolyte fabrication. Two of them are machined by a laser cutter in a grate-like shape. The third one is then sandwiched symmetrically between two grate type thin electrolytes. After isostatic pressing at 40 MPa for 10 min, grate type electrolyte is subjected to two stages sintering as the same as that applied for the base cell electrolyte.

Three different grate type electrolytes belonging to Cell A–C are designed and fabricated. Their technical drawings and photos after the lamination step are given in Fig. 2. Since the cells are designed as electrolyte supported, grate type electrolytes should have an adequate strength for both cell and stack applications even during sintering and coating of electrodes. Therefore, to avoid possible electrolyte failure, the volume ratio of subtracted parts to two layered ScCeSZ electrolyte laminate which corresponds to the reduced electrolyte area is kept as 10, 18 and 30% for Cell A–C, respectively. In other words, although the thickness of the electrolyte for the base cell is around 150 μm, the electrolyte thickness in the active area is only around 50 μm for 18% of Cell A, 28% of Cell B and 40% of Cell C. The photos of the sintered electrolytes belonging to Cell A–C are given in Fig. 3.

2.1.3. Fabrication of electrodes

NiO–F powders (Novamet, New Jersey, USA) are mixed with ScCeSZ powders corresponding to a weight ratio of 3:2, respectively. An appropriate amount of ethyl cellulose binder and terpineol solver (both from Sigma–Aldrich, Munich, Germany) is also added to prepare a printable AFL ink. No pore former is added to the AFL screen printing solution of the base cell. After ball milling for around 12 h and homogenization via a three rolls mill, the ink is first brush painted into channels of the electrolyte in order to assure the uniform anode thickness after the screen printing and

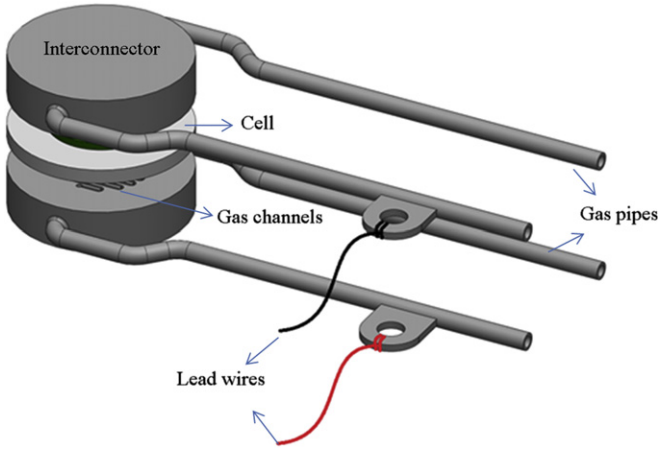

Fig. 4. Short stack configuration for the performance measurements.

increase the TPBs. Then screen printing of AFL is applied. Before the printing of the ACL layer, AFL layer is dried in a furnace at 100 °C for 30 min. The screen printing paste for the ACL layer is prepared similarly. High purity green NiO–A powders (Novamet) are mixed with ethyl cellulose and terpineol at suitable ratios. No ScCeSZ is used in the ACL layer, since only the electronic conductivity is the issue. In contrast to AFL paste, activated charcoal (Sigma–Aldrich) is also added as a pore former at a weight of 10 wt. % of NiO–A powders. After ball milling for around 12 h and homogenization via a three rolls mill, the ACL paste is screen printed on the AFL dried at 100 °C. Both anode layers are then co-sintered at 1250 °C for 3 h. The thicknesses of the AFL and ACL can be controlled mainly by the number of the passes performed by the printing machine. AFL and overall anode thickness from the uncoated electrolyte surface are measured as 20 μm and 30 μm, respectively indicating that ACL is 10 μm thick. The active anode area is adjusted to 11.62 cm^2 (3.85 cm in diameter) for all cell fabricated. Similarly, LSF ($La_{0.60}Sr_{0.40}FeO_{3-d}$, Nextech Materials)/ScCeSZ (wt. % 50/50) cathode functional layer and LSF cathode current collecting layer are coated on the other side of the electrolyte symmetric to the anode with the same active area of 11.62 cm^2. After co-sintering of both cathode layers at 1000 °C for 2.5 h, all cells are then ready for

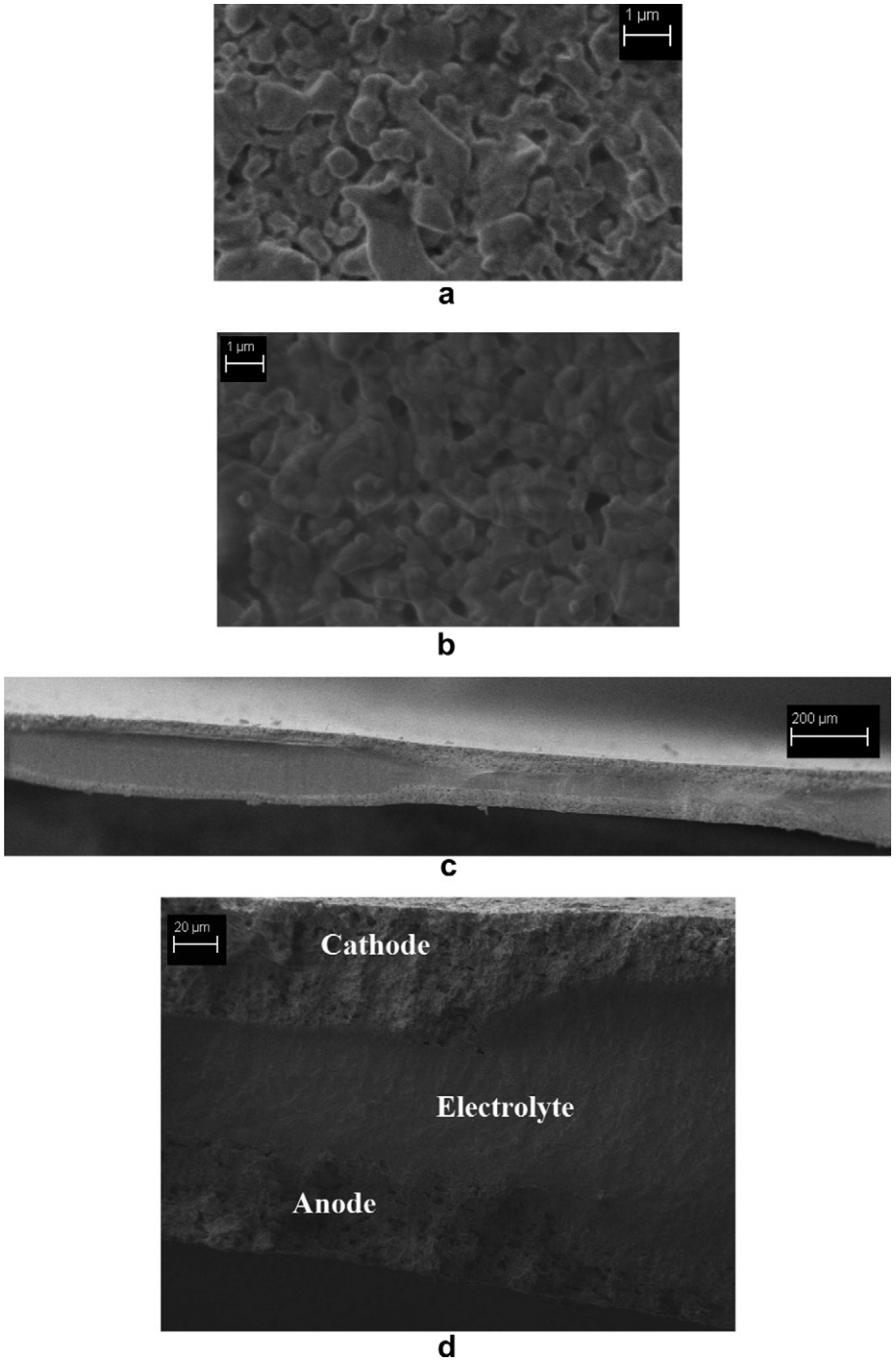

Fig. 5. Scanning electron micrographs of the cathode (a), the anode (b), cross-section (c) and detailed cross-section (d) of Cell A.

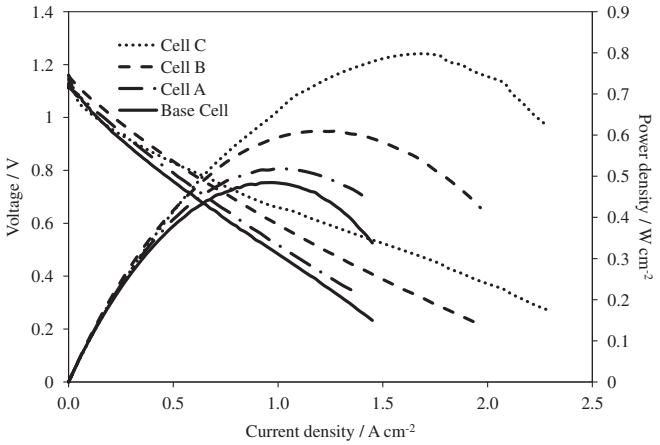

Fig. 6. I–V and I–P characteristics of cells at 750 °C.

testing. The thicknesses of the cathode layers are the same as those of corresponding anode layers.

2.2. Cell characterization

Fabricated single cells are inserted between two stainless steel interconnectors for the performance measurements as shown in Fig. 4. Silver ink (Nextech Materials) is applied as a current collecting paste for both electrodes. Then cells are placed in a temperature controlled furnace connected to the fuel cell test station (Arbin Instruments, FCTS, Texas, USA). The furnace has also a push rod pressing capability for better current collection. The current and voltage sensing probes of the test station are mounted directly to the gas pipes welded to the interconnectors.

The test station allows the user to control gas flow rates with humidification if demanded. The anode side of cells is firstly purged with nitrogen until the operation temperature is reached and then reduced by hydrogen for half an hour. The cell performance is measured from 700 to 800 °C with hydrogen as a fuel and air as an oxidant. The microstructural properties of the cells are investigated via a scanning electron microscope (Carl Zeiss, Evo 40, London, England) while impedance measurements are through an impedance analyzer (Solartron Analytical, 1260A, Hempshire, UK) in a frequency range of 0.1 Hz–250 kHz.

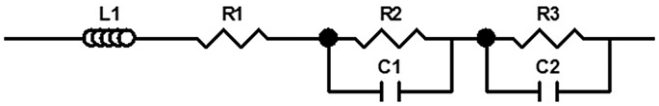

Fig. 8. The equivalent circuit for fitting the measured impedance.

3. Result and discussion

3.1. Microstructure

The microstructural images captured from Cell A are shown Fig. 5. It is seen that both electrodes are porous as expected and well bonded to the electrolyte. No formation of secondary phases is visible between the electrolyte and both electrodes. The electrolyte has crack and delamination free dense structure even the thin parts. SEM investigations showed that it is possible to fabricate dense electrolyte with locally reduced thickness without any cracks.

3.2. Cell characterization

The performance comparison of cells tested at 750 °C is illustrated in Fig. 6. The performance of the base cell is also given in the figure for comparison. It is seen that all novel structured electrolytes show higher performance than the base cell and the improvement in the performance increases from Cell A to Cell C with the increasing the percent of thin electrolyte in the active area. Among them, Cell C having the highest percent of thin electrolyte in the active region showed the highest peak power density as 0.8 W cm^{-2} (9.27 W) as expected while the base cell exhibits only 0.485 W cm^{-2} (5.64 W).

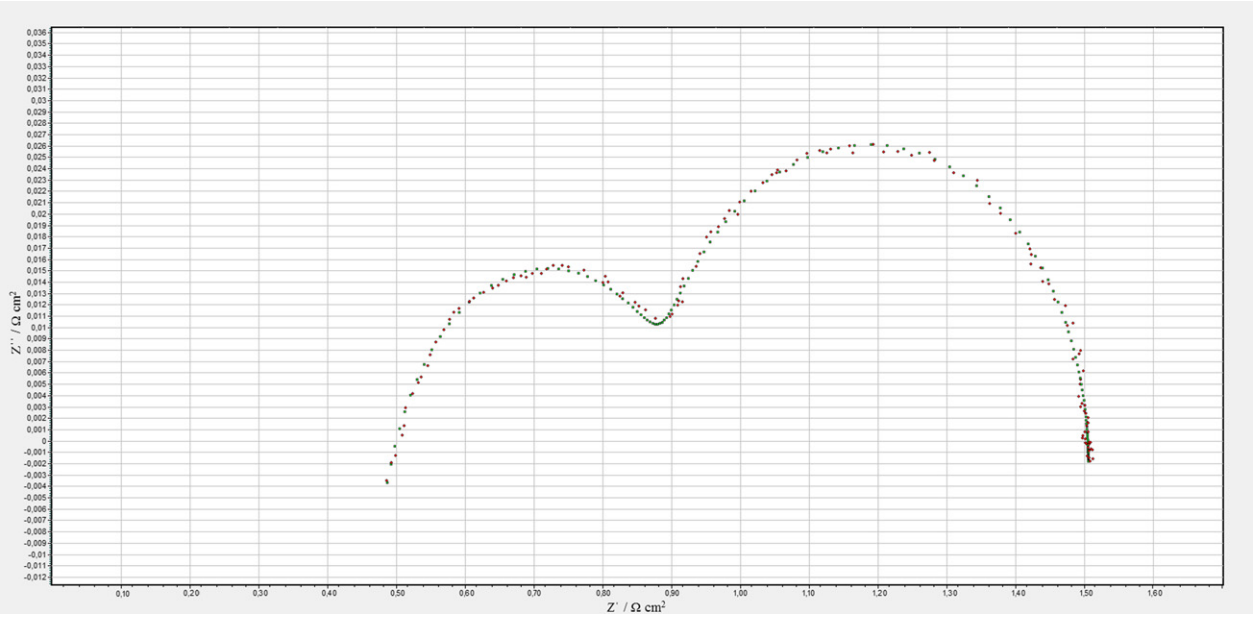

Fig. 7. Impedance result of the base cell at 750 °C.

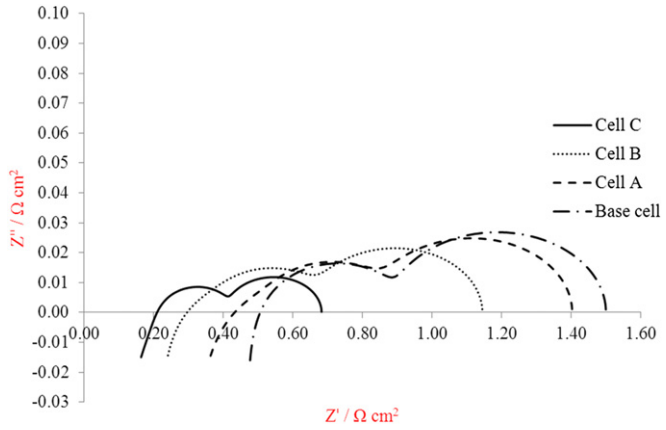

Fig. 9. Impedance comparison of cells A–C and the base cell at 750 °C.

The impedance result of the base cell at 750 °C is given in Fig. 7. The red squares stand for the experimental data while the green ones are the fitted values obtained from the equivalent circuit consisting of an inductor, a resistance and two RC parallel circuits as given in Fig. 8. The two RC parallel circuits correspond to the electrode impedances including the reaction resistances on both electrodes and the interfacial capacitances between the both electrodes and the electrolyte whereas the resistance (R_1) corresponds to the ohmic resistance of the cell. The inductor (L), on the other hand, is due to the metallic interconnectors and leads. The fitted impedance results obtained from all cells at 750 °C are given in Fig. 9. The ohmic resistance of the cells tends to decrease with the increasing the percent of thin electrolyte in the active region although the ohmic contribution of both electrodes is expected to increase since more electrode materials is required to fill the channels on the electrolyte. Similarly, the polarization resistance of both electrodes also decreases from the base cell to Cell C. Thus, the results indicate that the improvement in the performance is mainly due to both the reduction in the electrolyte resistance and increased number of the three phase boundaries achieved by the novel electrolyte design proposed.

The performance of the Cell C which exhibits the highest performance is shown in Fig. 10. The cell shows 0.52, 0.8 and 1.26 W cm^{-2} peak power at densities at 700, 750 and 800 °C operation temperature, respectively. Furthermore, the base cell at 840 °C shows almost the same power output as exhibited by the Cell C at an operation temperature of 750 °C indicating that the novel electrolyte design of Cell C also offers about a significant amount of reduction in the operation temperature as well.

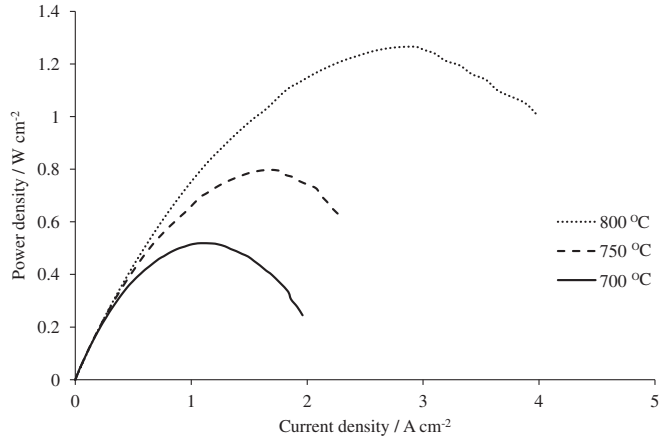

Fig. 10. Performance of Cell C at different operation temperatures.

4. Conclusions

Three different ScCeSZ-based electrolytes having grate-like structure with various percent of partly reduced thickness are designed and fabricated to improve the cell performance as well as to lower the operation temperature. Performance measurements showed that Cell C having 40 percent of thin electrolyte has the highest peak power at all operation temperatures studied. Impedance results indicated that the improvement in the performance is as a result of the reduction in the electrolyte resistance due to partly reduced electrolyte thickness in the active cell area and increased number of the three phase boundaries. Furthermore, 0.8 W cm^{-2} is obtained from Cell C at an operation temperature of 750 °C whereas the base cell shows the same power density at around 840 °C. Thus, the proposed design also offers a reduction in the operation temperature around 100 °C which possibly allows reducing the operational cost and startup/shut down periods of the SOFC systems.

References

[1] S.C. Singhal, Solid State Ionics 135 (2000) 305–313.
[2] S.H. Chan, X.J. Chen, K.A. Khor, Solid State Ionics 158 (2003) 29–43.
[3] J. Ma, T.S. Zhang, L.B. Kong, P. Hing, S.H. Chan, J. Power Sources 132 (2004) 71–76.
[4] K.A. Khor, L.G. Yu, S.H. Chan, X.J. Chen, J. Eur. Ceram. Soc. 23 (2003) 1855–1863.
[5] Y. Du, N.M. Sammes, J. Eur. Ceram. Soc. 21 (2001) 727–735.
[6] N.M. Sammes, G.A. Tompsett, H. Nafe, F. Aldinger, J. Eur. Ceram. Soc. 19 (1999) 1801–1826.
[7] D.S. Lee, W.S. Kim, S.H. Choi, J. Kim, H.W. Lee, J.H. Lee, Solid State Ionics 176 (2005) 33–39.
[8] S. Komine, T. Iimure, E. Iguchi, Solid State Ionics 176 (2005) 2535–2543.
[9] K. Chen, Z. Lu, N. Ai, X. Huang, Y. Zhang, X. Xin, R. Zhu, W. Su, J. Power Sources 160 (2006) 436–438.
[10] Y. Zhang, X. Huang, Z. Lu, Z. Liu, X. Ge, J. Xu, X. Xin, X. Sha, W. Su, J. Power Sources 158 (2006) 1048–1050.
[11] T. Inagaki, F. Nishiwaki, J. Kanou, S. Yamasaki, K. Hosoi, T. Miyazawa, M. Yamada, N. Komada, J. Alloys Compd. 408-412 (2006) 512–517.
[12] X. Xin, Z. Lu, X. Huang, X. Sha, Y. Zhang, W. Su, J. Power Sources 159 (2006) 1158–1161.
[13] M. Sahibzada, B.C.H. Steele, K. Zheng, R.A. Rudkin, I.S. Metcalfe, Catal. Today 38 (1997) 459–466.
[14] B. Zhu, I. Albinsson, C. Andersson, K. Borsand, M. Nilsson, B.E. Mellander, Electrochem. Commun. 8 (2006) 495–498.
[15] Y.J. Leng, S.H. Chan, K.A. Khor, S.P. Jiang, P. Cheang, J. Power Sources 117 (2003) 26–34.
[16] G. Meng, H. Song, Q. Dong, D. Peng, Solid State Ionics 175 (2004) 29–34.
[17] Y. Yoo, J. Power Sources 160 (2006) 202–206.
[18] B. Timurkutluk, C. Timurkutluk, M.D. Mat, Y. Kaplan, Int. J. Energy Res. (2011). doi:10.1002/er.1921.
[19] S. Sarat, N.M. Sammes, A. Smirnova, J. Power Sources 159 (2006) 1158–1161.
[20] X.J. Ning, C.X. Li, C.J. Li, G.Y. Yang, Vacuum 80 (2006) 1261–1265.
[21] T. Matsui, M. Inaba, A. Mineshige, Z. Ogumi, Solid State Ionics 176 (2005) 647–654.
[22] B. Timurkutluk, C. Timurkutluk, M.D. Mat, Y. Kaplan, J. Power Sources 196 (2011) 9361–9364.
[23] O.A. Marina, C. Bagger, S. Primdahl, M. Mogensen, Solid State Ionics 123 (1999) 199–208.
[24] M. Mogensen, N.M. Sammes, G.A. Tompsett, Solid State Ionics 129 (2000) 63–94.
[25] F.F. Lange, G.L. Dunlop, B.I. Davis, J. Am. Ceram. Soc. 69 (1986) 237–240.
[26] N. Claussen, J. Am. Ceram. Soc. 59 (1976) 49–51.
[27] S.E. Dougherty, T.G. Nieh, J. Wadsworth, Y. Akimune, J. Mater. Res. 10 (1995) 113–118.
[28] Z. Wang, M. Cheng, Z. Bi, Y. Dong, H. Zhang, J. Zhang, Z. Feng, C. Li, Mater. Lett. 59 (2005) 2579–2582.
[29] N. Orlovskaya, S. Lukich, G. Subhash, T. Graule, J. Kuebler, J. Power Sources 195 (2010) 2774–2781.
[30] K. Du, C. Kim, A. Heuer, J. Am. Ceram. Soc. 91 (2008) 1626–1633.
[31] A. Faes, J.M. Fuerbringer, D. Mohamedic, A.H. Wysera, G. Cabochec, J. Van Herle, J. Power Sources 196 (2011) 7058–7069.
[32] P. Blennow, A. Hagen, K.K. Hansen, L.R. Wallenberg, M. Mogensen, Solid State Ionics 179 (2008) 2047–2058.

[33] Q. Ma, F. Tietz, A. Leonide, E.I. Tiffée, Electrochem. Commun. 12 (2010) 1326–1328.
[34] Y. Bai, C. Wang, J. Ding, C. Jin, J. Liu, J. Power Sources 195 (2010) 3882–3886.
[35] J. Ding, J. Liu, J. Power Sources 193 (2009) 769–773.
[36] Y. Zhang, J. Liu, J. Yin, W. Yuan, J. Sui, Int. J. Appl. Ceram. Technol. 5 (2008) 568–573.
[37] T. Suzuki, B. Liang, T. Yamaguchi, K. Hamamoto, Y. Fujishiro, Electrochem. Commun. 13 (2011) 719–722.
[38] J. Park, J. Bae, Y.K. Kim, Int. J. Hydrogen Energy 36 (2011) 9936–9944.
[39] M. Suzuki, N. Shikazono, K. Fukagata, N. Kasagi, J. Power Sources 180 (2008) 29–40.
[40] H. Zhong, H. Matsumoto, T. Ishihara, A. Toriyama, J. Power Sources 186 (2009) 238–243.
[41] H. Zhong, H. Matsumoto, T. Ishihara, A. Toriyama, Solid State Ionics 179 (2008) 1474–1477.
[42] T. Yamaguchi, S. Shimizu, T. Suzuki, Y. Fujishiro, M. Awano, Mater. Lett. 63 (2009) 2577–2580.
[43] J.J. Hwang, C.K. Chen, D.Y. Lai, J. Power Sources 143 (2005) 75–83.
[44] Y. Yang, G. Wang, H. Zhang, W. Xia, J. Power Sources 173 (2007) 233–239.
[45] Y. Yang, G. Wang, H. Zhang, W. Xia, J. Power Sources 177 (2008) 426–433.
[46] F.J. Gardner, M.J. Day, N.P. Brandon, M.N. Pashley, M. Cassidy, J. Power Sources 86 (2000) 122–129.
[47] P. Costamagna, S. Selimovic, M.D. Borghi, G. Agnew, Chem. Eng. J. 102 (2004) 61–69.
[48] B.A. Haberman, J.B. Young, Int. J. Heat Mass Transfer 47 (2004) 3617–3629.